SPEKTRA: Jurnal Fisika dan Aplikasinya
Volume 11, Issue 2, August 2026
Homepage: doi.org/10.21009/SPEKTRA

DOI: doi.org/10.21009/SPEKTRA.112.05

Magnitude Transformation from RGB Bayer Filter to the Johnson-Cousins BVR Filter Based on CAT-ITB Telescope Photometric Observations of Selected Open Clusters

Raihan Amirul Husana[1,*], Mahasena Putra[2], Anton Timur Jaelani[2], Chatief Kunjaya[2], Aliyya Nur Rahma[3], Firdaus Orvin Dwifauja Manalu[1]

[1]*Astronomy Study Program, FMIPA, Institut Teknologi Bandung, Jl. Ganesa 10, Bandung 40132, Indonesia*
[2]*Astronomy Research Group, FMIPA, Institut Teknologi Bandung, Jl. Ganesa 10, Bandung 40132, Indonesia*
[3]*Astronomy Doctoral Program, FMIPA, Institut Teknologi Bandung, Jl. Ganesa 10, Bandung 40132, Indonesia*

*Corresponding Author Email: hansamirul@gmail.com

Received: 29 June 2026
Revised: 10 August 2026
Accepted: 28 August 2026
Online: 30 August 2026
Published: 30 August 2026

SPEKTRA: Jurnal Fisika dan Aplikasinya
p-ISSN: 2541-3384
e-ISSN: 2541-3392

ABSTRACT

Photometry is one of the astronomical measurement methods that provides astronomers with information about the brightness of astronomical objects at various wavelengths. Over time, various photometric systems have been developed. Therefore, transformations are necessary to convert results from one photometric system to another, with the aim of facilitating scientific communication among researchers working with various photometric systems. The CAT-ITB, or City Astronomical Telescope ITB, is an 11-inch optical telescope located at CAS ITB, equipped with detectors, one of which is the ZWO ASI 183MC that uses the RGB Bayer filter. Hence, transformation equations from the RGB Bayer filter system to the Johnson-Cousins BVR filter system must be established. By utilizing transformation equations that have historically been widely used by previous researchers, this study focuses on deriving the coefficients needed to solve those equations. Observational data of open clusters M67, RU 135, IC 4665, and M11 were obtained using CAT-ITB, which were used to optimize the transformation equations. The coefficients derived from M67 photometric data yielded the best results. The total RMS values for the magnitude transformations of clusters M67, RU 135, IC 4665, and M11 in each of the $B_{Johnson}$, $V_{Johnson}$, and $R_{Cousins}$ conversions are 0.296, 0.152, and 0.161 respectively. All transformations produced small residuals and colour-magnitude diagrams that closely resemble those from catalog data. This study contributes a validated set of transformation coefficients and zero-point constants specific to the

CAT-ITB RGB Bayer detector system, offering a practical reference for converting RGB-based photometric observations into the standard Johnson-Cousins system for future small-telescope and citizen-science photometric research.

Keywords: Photometry, Transformation, RGB Bayer Filter, Johnson-Cousins BVR Filter, Open Cluster

INTRODUCTION

Photometry measures the brightness of celestial objects, given in magnitudes, in many wavelength regions. Over the years, different observers have developed many photometric systems with a variety of detectors and passbands that can be classified into broad band $(400\text{Å} < \Delta\lambda < 1000\text{ Å})$, intermediate band $(70\text{ Å} < \Delta\lambda < 400\text{ Å})$, and narrow band $(\Delta\lambda < 70\text{ Å})$ systems [1, 2]. This research focuses on filters from broad band photometric system, specifically the RGB Bayer system and the Johnson-Cousins BVR system.

The RGB Bayer filter is a very common system that has been used by scientific and commercial cameras [3-5]. Previous studies have established that these RGB cameras are valuable for brightness measurements [3-6]. However, there is no consistent magnitude system that has been defined for the RGB system. Therefore, converting between different systems is required to facilitate communication among astronomers using various filter sets, including RGB filters. Meanwhile, the Johnson-Cousins UBVRI system is one of the most common systems used by astronomers, with many previous studies having been conducted [1, 7-10]. Therefore, transformation from the RGB Bayer filter system into the Johnson-Cousins BVR filter system can be valuable for scientific development.

Reliable transformation equations from previous research are used in this study [5, 11, 12]; these equations can be seen below:

$$
\begin{aligned}
B_J &= B_{B,ZP} + B_B + C_{B,BG}(B_B - G_B) + C_{B,GR}(G_B - R_B) \\
V_J &= G_{B,ZP} + G_B + C_{V,BG} + (B_B - G_B) + C_{V,GR}(G_B - R_B) \\
R_C &= R_{B,ZP} + C_{R,BG}(B_B - G_B) + C_{R,GR}(G_B - R_B)
\end{aligned}
\tag{1}
$$

with B_J, V_J, and R_C as magnitudes in the Johnson-Cousins BVR system, while B_B, G_B, and R_B are magnitudes in the RGB Bayer system. Constants with the subscript ZP are zero-points for the RGB system. The zero-point constants value are dependent on atmosphere and other observing conditions. While the rest of coefficients are transformation coefficients.

Therefore, this study aims to derive and evaluate transformation coefficients that convert RGB Bayer magnitudes obtained from CAT-ITB observations into the Johnson-Cousins BVR photometric system, using photometric data of the open clusters M67, RU 135, IC 4665, and M11, and to assess the reliability of the resulting transformation through comparison with catalogue magnitudes.

TABLE 1. Observation log for the targeted objects

Date	Object	Exposure Time	RA	Dec	Altitude
27 April 2025	RU 135	25 s	$17_h\ 58_m\ 03_s$	−11°40′37″	82.548°
28 April 2025	M11	5 s	$18_h\ 51_m\ 06_s$	-06°16′00″	72.720°
28 April 2025	M67	10 s	$08_h\ 51_m\ 24_s$	+11°49′00″	42.113°
30 April 2025	IC 4665	5 s	$17_h\ 46_m\ 12_s$	+05°43′00″	63.237°

METHOD

Observations and Data Reduction

Observations were conducted using the CAT-ITB, which is sited in the ITB college building, and equipped with RASA 11 optical tube assembly [13] and ZWO ASI 183 MC RGB camera [14]. Each of the RGB Bayer filters in the camera has an effective wavelength of 5900 Å, 5300Å, and 4600 Å, with RGGB filter pattern [14, 15]. Different open clusters were used as primary objects due to their characteristics, providing stars with a wide range of colours and magnitudes [16]. Objects for the observation were chosen based on the available database on the Johnson-Cousins BVR and the RGB Bayer filter, such as M67, M11, IC 4665, and RU 135 [17-23]. The RGB Bayer magnitudes will be obtained from the observations, while the Johnson-Cousins BVR magnitudes will be obtained from the available database. Main-sequence stars and non-variable stars, including standard stars, were selected and cross-checked based on the stars' coordinates with other databases to be used for analysis [17-29].

Observations were performed from April 27th to April 30th 2025 during midnights with ideal observation condition. Bias and dark calibration images were obtained on the same night as the observations, while sky flats were obtained during twilight at sunrise on April 30th. After basic calibration process was completed, 10 images of each object were mean-stacked to gain better signal-to-noise ratio (SNR). The observation log is presented in TABLE 1.

To minimize the atmospheric extinction effects, differential photometry was used to obtain the magnitudes. The stars were selected whenever these criteria are met: 1) Objects are not saturated; 2) Objects have an SNR higher than 10; and 3) Objects have 9 or more connected pixels to confirm that the source has a PSF profile. Then, all magnitudes were corrected for the reddening effect of interstellar matter [30-32].

Optimization

The value of each constant and coefficient in EQUATION (1) will be derived using an optimization process. The optimization will find the value of all the zero-point constants and transformation coefficients that minimizes the difference between the magnitudes obtained from the transformation process and the catalog magnitudes. EQUATION (1) is then rewritten as:

$$\Delta B^2 = \left(B_{B,ZP} + B_B + C_{B,BG}(B_B - G_B) + C_{B,GR}(G_B - R_B) - B_J\right)^2 \approx 0,$$
$$\Delta V^2 = \left(G_{B,ZP} + G_B + C_{V,BG}(B_B - G_B) + C_{V,GR}(G_B - R_B) - V_J\right)^2 \approx 0, \quad (2)$$
$$\Delta R^2 = \left(R_{B,ZP} + R_B + C_{R,BG}(B_B - G_B) + C_{R,GR}(G_B - R_B) - R_C\right)^2 \approx 0,$$
$$\text{Total} = \Delta B^2 + \Delta V^2 + \Delta R^2 \approx 0.$$

The value of zero-point constants and transformation coefficients is then used to transform the RGB magnitudes into the BVR magnitudes, followed by sigma clipping applied to the results with the least-square error higher than 2.5σ. These processes are then repeated two times, except if the transformation results already have the lowest Root Mean Square (RMS) error before the next iterative process. Note that this process was implemented on all of the open clusters used in this research one by one.

Each set of transformation coefficients from one cluster is then applied to transform the other cluster RGB Bayer magnitudes. Since the zero-point constants represent the condition of the observation, the constants were derived again with the same iterative optimization process to each object being transformed. These processes are implemented on all observed clusters and the RMS errors for each transformation was summed. The total RMS error of applying transformation coefficient from one cluster is then compared to the other cluster's results to find which coefficient is best used for magnitude transformation.

RESULT AND DISCUSSION

The final results of the optimization process can be found in TABLE 2. Each cluster yields different values for each transformation coefficient. This is most likely caused by the different range of colours of the clusters and also its distribution as illustrated in FIGURE 1. Though some stars in one cluster are similar to other stars from the other clusters, indicated by the overlapping bar, the values of each transformation coefficient vary.

TABLE 2. Transformation coefficients derived from the optimization process for each observed cluster

Coefficients	M67	M11	IC 4665	RU 135
$C_{B,BG}$	-0.083	-0.589	-0.007	-0.660
$C_{B,GR}$	0.737	0.867	0.955	1.025
$C_{V,BG}$	0.166	0.044	0.224	-0.126
$C_{V,GR}$	-0.002	0.255	-0.055	0.155
$C_{R,BG}$	-0.315	-0.144	-0.158	-0.316
$C_{R,GR}$	0.529	0.729	0.326	0.551

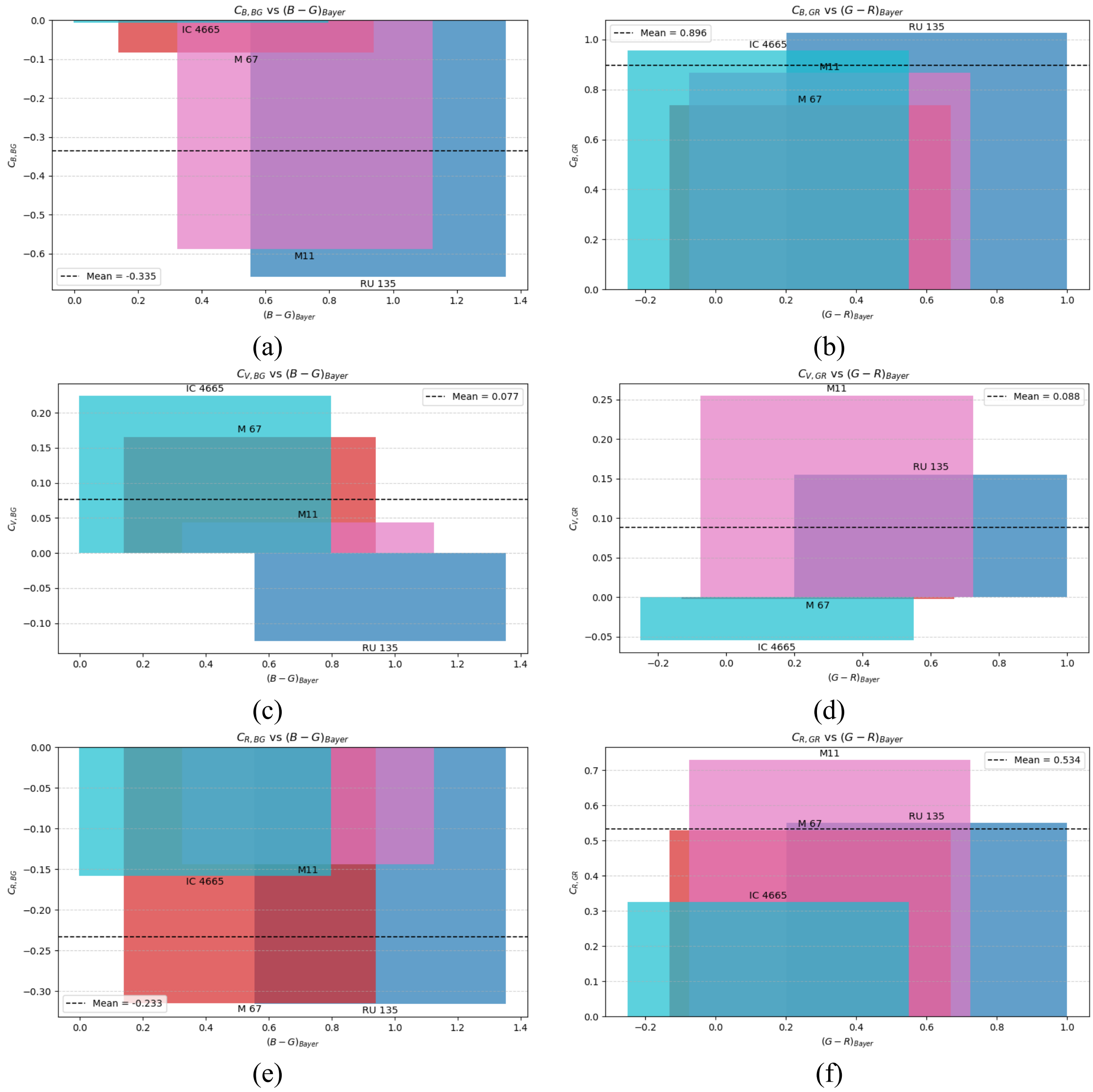

FIGURE 1. Histogram showing the relationship between the colour distribution of observed data and the derived transformation coefficients value with the dashed line represents the mean of every value. Figure (a) shows the relation between $(B-G)_{Bayer}$ colour and $C_{B,BG}$ coefficients. Figure (b) shows the relation between $(G-R)_{Bayer}$ colour and $C_{B,GR}$ coefficients. Figure (c) shows the relation between $(B-G)_{Bayer}$ colour and $C_{V,BG}$ coefficients. Figure (d) shows the relation between $(G-R)_{Bayer}$ colour and $C_{V,GR}$ coefficients. Figure (e) shows the relation between $(B-G)_{Bayer}$ colour and $C_{R,BG}$ coefficients. Figure (f) shows the relation between $(G-R)_{Bayer}$ colour and $C_{R,GR}$ coefficients

Based on the application from each cluster to one another, the transformation conducted using coefficients derived from M67 observed data produced the best results with the lowest total RMS, while coefficients derived from M11 observed data produced the highest RMS (TABLE 3). Therefore, coefficients derived from M67 will be used for further process. The zero-point constants derived using M67's transformation coefficients are listed on TABLE 4. Using the determined coefficients, the RMS error for transformation of M67 magnitudes are 0.081, 0.031, and 0.056 for B_J, V_J, and R_C transformation respectively. The RMS error for

TABLE 3. RMS value for each transformation

	B_J Transformation RMS	V_J Transformation RMS	R_C Transformation RMS	Total RMS
	Transformation using M67's derived coefficient			
M67	0.081	0.031	0.056	0.168
M11	0.072	0.058	0.054	0.184
IC 4665	0.039	0.021	0.025	0.085
RU 135	0.104	0.042	0.026	0.172
Total	**0.296**	**0.152**	**0.161**	**0.609**
	Transformation using M11's derived coefficient			
M67	0.098	0.041	0.056	0.195
M11	0.076	0.064	0.056	0.196
IC 4665	0.084	0.028	0.056	0.168
RU 135	0.090	0.046	0.050	0.186
Total	**0.348**	**0.179**	**0.218**	**0.745**
	Transformation using IC 4665's derived coefficient			
M67	0.084	0.029	0.051	0.164
M11	0.076	0.057	0.049	0.182
IC 4665	0.020	0.022	0.026	0.068
RU 135	0.122	0.045	0.030	0.197
Total	**0.302**	**0.153**	**0.156**	**0.611**
	Transformation using RU 135's derived coefficient			
M67	0.101	0.054	0.056	0.211
M11	0.081	0.066	0.055	0.202
IC 4665	0.075	0.030	0.026	0.131
RU 135	0.086	0.030	0.026	0.142
Total	**0.343**	**0.180**	**0.163**	**0.686**

TABLE 4. Zero-point constants derived from the optimization process using M67's coefficient results

Zero-points	M67	M11	IC 4665	RU 135
$B_{B,ZP}$	-0.229	−1.248	−0.455	−1.366
$G_{B,ZP}$	-0.111	−0.405	−0.102	−0.456
$R_{B,ZP}$	-0.013	0.089	0.109	0.097

transformation of M11 magnitudes are 0.072, 0.058, and 0.054 for B_J, V_J, and R_C transformation respectively. The transformation of IC 4665 magnitudes resulted in RMS errors of 0.039, 0.021, and 0.025 for B_J, V_J, and R_C transformation respectively, while the transformation of RU 135 has RMS value of 0.104, 0.042, and 0.026 for B_J, V_J, and R_C transformation respectively. As a comparison, a previous study reported IC 4665's transformation RMS of B_J, V_J, and R_C valued at 0.095, 0.094, and 0.070 respectively [5].

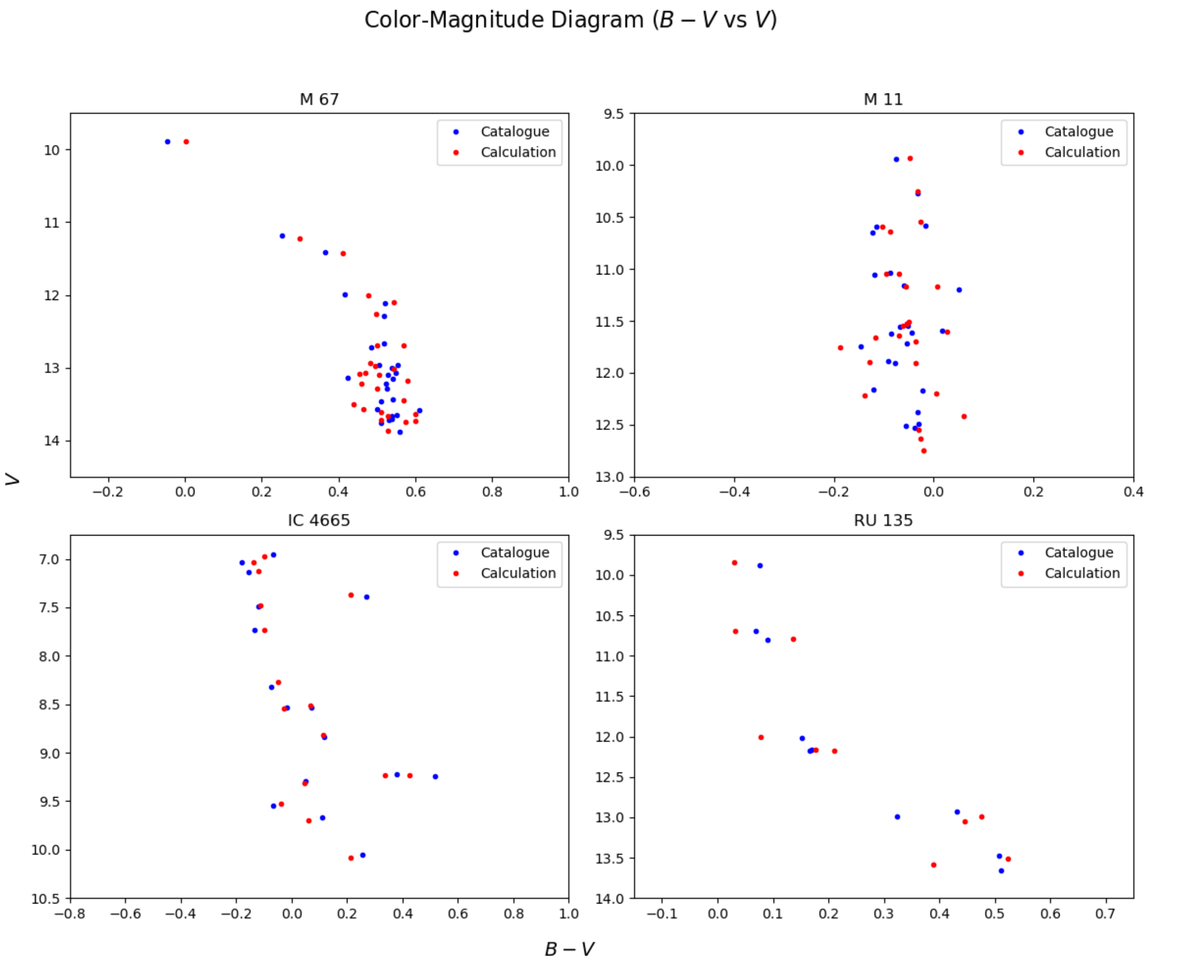

FIGURE 2. Overplot of the Colour-Magnitude Diagram ((B-V) vs V) of M67 (top left), M11 (top right), IC 4665 (bottom left), and RU 135 (bottom right). Each overplot compares the data obtained from catalogues and the result of transformation using coefficients derived from M67.

Almost every transformation result has smaller RMS error than the mentioned reference, which indicates that the transformations are reliable.

FIGURE 2 shows how the transformation using M67's coefficients produced a very close result compared to the catalogues. The residual of each cluster transformation also shows a small distribution, all lower than ±0.07 distribution for all filters, except the B_J transformation of RU 135 with 1σ valued at ±0.104 (FIGURE 3). Based on the residual plot, the data are more dispersed at higher magnitudes. There is also a pattern of B_J transformation having higher RMS and also higher residual distribution, which may indicate the effect of light pollution and atmospheric extinction.

The extinction effect is also indicated by the zero-point constants (TABLE 4). The zero-point constants value of B_J transformations have values further from zero, which means the results of B_J transformations have more deviation than the other filter transformations. This is in line with results from previous studies on the higher extinction effect at shorter wavelengths [33-35]. However, further research is needed to prove this hypothesis.

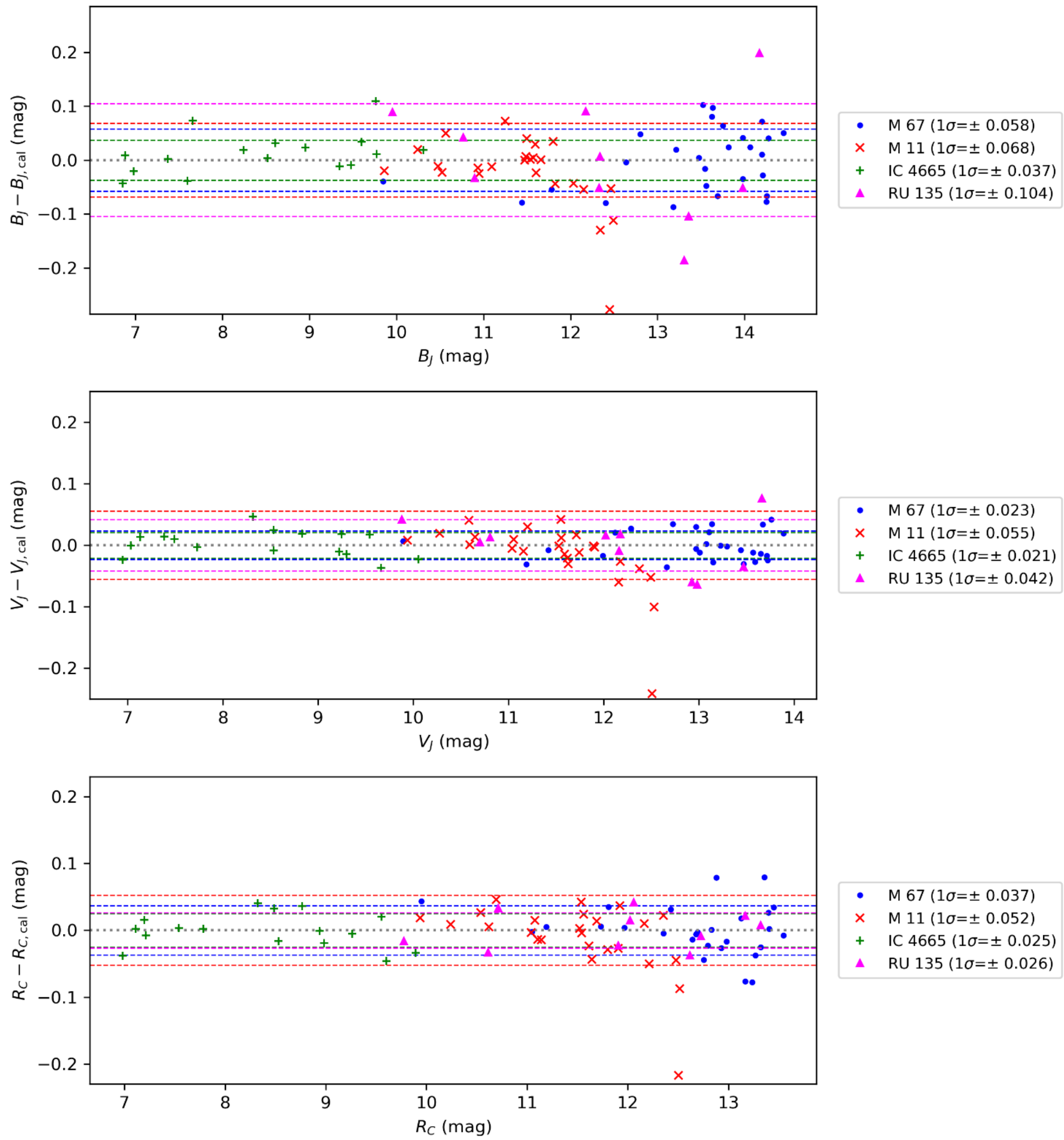

FIGURE 3. Residual plots for each B_J, V_J, and R_C magnitude transformation. The dashed line represents the distribution at 1σ of each open clusters transformation using coefficients derived from M67.

TABLE 4. Zero-point constants derived from the optimization process using M67's coefficient results

Zero-points	M67	M11	IC 4665	RU 135
$B_{B,ZP}$	-0.229	−1.248	−0.455	−1.366
$G_{B,ZP}$	-0.111	−0.405	−0.102	−0.456
$R_{B,ZP}$	-0.013	0.089	0.109	0.097

CONCLUSION

The transformation coefficient derived from M67 observed data is reliable and can be used for observation data obtained with CAT-ITB. Based on the application of the coefficients, these coefficients can be reliably used for main-sequence stars with a colour range of $-0.179 < B - V < 0.609$. Since the transformation coefficients are only used for main-sequence stars in three different clusters, further research is needed for stars with different colour ranges and evolution stages.

The value of transformation coefficients can also differ if they are derived from different clusters and if observed using different instruments, but the equation and the method can be used for future research.

This study also shows the pattern of higher error and deviation in B_J transformations, which can be caused by the observing conditions and the higher extinction effect at shorter wavelengths. Even though the observations were conducted in the middle of a city with light pollution, photometric observations can still be performed with desirable results if conducted on objects within the telescope limitations. In order to have better observational results, applying atmospheric extinction correction is recommended. Dimmer stars can also affect the transformation results. Therefore, reaching a higher SNR for the target object is also recommended.

The scientific contribution of this study lies in providing an empirically derived and validated set of transformation coefficients and zero-point constants specific to the CAT-ITB RGB Bayer detector system, obtained from multiple open cluster calibrators. This offers other researchers using RGB Bayer-filter instruments, particularly small and amateur telescopes located in urban, light-polluted environments, a practical and reproducible framework for converting RGB photometric measurements into the standard Johnson-Cousins BVR system, thereby broadening the range of instruments that can contribute reliable photometric data to the astronomical community.

ACKNOWLEDGMENTS

The authors would like to acknowledge the financial support provided by the PPMI FMIPA-ITB 2025 program (Number: 1Q/IT1.C02/KU/2025), which made this research possible.

REFERENCES

[1] M. Bessell, "Standard Photometric System," *Ann. Rev. Astron. Astrop.*, vol. 43, pp. 293–336, Sep. 2005. DOI: 10.1146/annurev.astro.41.082801.100251

[2] M. Catelan, "Stellar Variability in Ground-Based Photometric Surveys: An Overview," *Mem. Soc. Astr. Italiana*, vol. 94, Dec. 2023. DOI: 10.36116/MEMSAIT_94N4.2023.56

[3] N. Cardiel et al., "RGB Photometric Calibration of 15 Million Gaia Stars," *MNRAS*, vol. 507, pp. 318-329, Oct. 2021. DOI: 10.1093/mnras/stab2124

[4] J.M. Carrasco et al., "Photometric Catalogue for Space and Ground Night-Time Remote-Sensing Calibration: RGB Synthetic Photometry from Gaia DR3 Spectrophotometry," *Rem. Sens. 15*. Mar. 2023. DOI: 10.3390/rs15071767

[5] W. Park et al., "Photometric Transformation from RGB Bayer Filter System to Johnson-Cousins BVR Filter System," *ASR*, vol. 57, pp. 509-518, Jan. 2016. DOI: 10.1016/j.asr.2015.08.004

[6] N. Cardiel et al., "Synthetic RGB Photometry of Bright Stars: Definition of the Standard Photometric System and UCM Library of Spectrophotometric Spectra," *MNRAS*, vol. 504, pp. 3730–3748, Jul. 2021. DOI: 10.1093/mnras/stab997

[7] A. U. Landolt, "Comments on Optical Photometry and the Generation of Standard Stars," *ASP: Conf. Ser.,* vol. 503, pp. 13-24. 2016.

[8] A. U. Landolt, "UBVRI Photometric Standard Stars in the Magnitude Range 11.5 < V < 16.0 Around the Celestial Equator," *The Astro. J.*, vol. 104, Jul. 1992. DOI: 10.1086/116242

[9] A. U. Landolt, "UBVRI Photometric Standard Stars Around the Celestial Equator: Updates and Additions," *The Astro. J.*, vol. 137, pp. 4186–4269, May 2009. DOI: 10.1088/0004-6256/137/5/4186

[10] T. T. Moon, "Southern Clusters for Standardizing CCD Photometry," *JAAVSO*, vol. 45, pp. 86-91, Jun. 2017.

[11] K. Mamenec, "Transformation of DSLR Magnitudes to Standard Photometric System," *OEJV*, vol. 243, pp. 1–12, Dec. 2023. DOI: 10.5817/OEJV2023-0243

[12] F. Della Prugna, "Astronomical Tests of a Medium Format Digital Camera on a Large Schmidt Telescope," *Rev. Mex Astron. Astrop*, vol. 60, pp. 121–124, Apr. 2024. DOI: 10.22201/ia.01851101p.2024.60.01.09

[13] *Rowe Ackermann Schmidt Astrograph 11 v2 Manual*, Celestron, Torrance, CA. 2019.

[14] *ZWO ASI183MC Manual*, Suzhou ZWO CO, Suzhou, China. 2021.

[15] M. Z. Aprianizar, "City Astronomical Telescope ITB (CAT-ITB) – Pengembangan Sistem Observasi Semi-Robotik untuk Penelitian Objek Transien dan Color Magnitude Diagram Gugus Terbuka," Undergraduate Thesis, Dept. Astronomy, Ins. Teknologi Bandung, Bandung, Indonesia, 2024.

[16] B. W. Carroll and D. A. Ostlie, "Main Sequence and Post-Main-Sequence Stellar Evolution" in *An Introduction to Modern Astrophysics*, 2nd ed. Cambridge, U.K.: Cambridge University Press, 2017, pp. 475-476.

[17] AAVSO. (2024). *Standard fields* [Online]. Available: https://apps.aavso.org/vsd/stdfields

[18] I. Akkaya et al., "CCD UBVRI Photometry of the Galactic Open Clusters: BE 89, RU 135, and BE 10," *Rev. Mex Astron. Astrop.,* vol. 46, pp. 385–430, Oct. 2010. DOI: 10.48550/arXiv.1008.2867

[19] J. W. Menzies and F. Marang, "UBV(RI)C Observations of Johnson's Standard Sequence in IC 4665," *MNRAS*, vol. 282, pp. 313–316, Sep. 1996. DOI: 10.1093/mnras/282.2.313

[20] WEBDA. (2024). *WEBDA page for open cluster IC 4665* [Online]. Available: https://webda.physics.muni.cz/cgi-bin/ocl_page.cgi?dirname=ic4665

[21] WEBDA. (2024). *WEBDA page for open cluster NGC 6705* [Online]. Available: https://webda.physics.muni.cz/cgi-bin/ocl_page.cgi?dirname=ngc6705

[22] WEBDA. (2024). *WEBDA page for open cluster NGC 2682* [Online]. Available: https://webda.physics.muni.cz/cgi-bin/ocl_page.cgi?dirname=ngc2682

[23] WEBDA. (2024). *WEBDA page for open cluster RU 135* [Online]. Available: https://webda.physics.muni.cz/cgi-bin/ocl_page.cgi?dirname=ru135

[24] L. Casamiquela et al., "NGC 6705: A Young α-Enhanced Open Cluster from OCCASO Data," *A&A*, vol. 610, Mar. 2018. DOI: 10.1051/0004-6361/201732024

[25] A. M. Geller et al., "Stellar Radial Velocities in the Old Open Cluster M67 (NGC 2682). II. The Spectroscopic Binary Population," *The Astro. J.*, vol. 161, Apr. 2021. DOI: 10.3847/1538-3881/abdd23

[26] G. Gonzalez, "Variability Among Stars in the M67 Field from Kepler/K2 Campaign-5 light Curves," *MNRAS,* vol. 459, pp. 1060–1068, Jun. 2016. DOI: 10.1093/mnras/stw700

[27] J. H. Peña et al., "Physical Properties and Membership Determination of the Open Clusters IC 4665, NGC 6871 and DZIM 5 Through ubvy−β Photoelectric Photometry," *Rev. Mex Astron. Astrop.*, vol. 59, pp. 45–65, Apr. 2023. DOI: 10.22201/ia.01851101p.2023.59.01.03

[28] T. Pribulla et al., "MOST Satellite Photometry of Stars in the M67 Field: Eclipsing Binaries, Blue Stragglers and δ Scuti Variables," *MNRAS*, vol. 391, pp. 343–353, Nov. 2008. DOI: 10.1111/j.1365-2966.2008.13889.x

[29] E. L. Sandquist et al., "The K2 M67 Study: A Curiously Young Star in an Eclipsing Binary in an Old Open Cluster," *The Astro. J.*, vol. 155, Apr 2018. DOI: 10.3847/1538-3881/aab0ff
[30] J. A. Cardelli et al., "The Relationship between Infrared, Optical, and Ultraviolet Extinction," *The Astro. J.*, vol. 345, pp. 245–256, Oct. 1989. DOI: 10.1086/167900
[31] E. L. Fitzpatrick et al, "An Analysis of the Shapes of Interstellar Extinction Curves. VII. Milky Way Spectrophotometric Optical-Through-Ultraviolet Extinction and Its R-dependence," *The Astro. J.*, vol. 886, Dec. 2019. DOI: 10.3847/1538-4357/ab4c3a
[32] F. Yi, et al., "Empirical Extinction Coefficients for the Swift-UVOT Optical-Through-Ultraviolet Passbands", *MNRAS*, vol 525, pp 2701–2707, Oct. 2023. DOI: 10.1093/mnras/stad2463
[33] M. F. Aboushelib et al., "UBVRI Night Sky Brightness at Kottamia Astronomical Observatory," in *Sci. Rep. 13*, Oct. 2023. DOI: 10.1038/s41598-023-43844-x
[34] M. Yusuf et al., "Atmospheric Extinction Coefficients and Night Sky Brightness at Bosscha Observatory," *J. Phys.: Conf. Ser.*, vol. 2773, 2024. DOI: 10.1088/1742-6596/2773/1/012003
[35] M. Yusuf et al., "Atmospheric Extinction Coefficients and Night Sky Brightness at ITB-Undana Remote Telescope Site," *J. Phys.: Conf. Ser.*, vol. 2773, 2024. DOI: 10.1088/1742-6596/2773/1/012005